

## Characterizing the Water Wire in the Gramicidin Channel Found by Monte Carlo Sampling Using Continuum Electrostatics and in Molecular Dynamics Trajectories with Conventional or Polarizable Force Fields

Yingying Zhang<sup>\*,†</sup>, Kamran Haider<sup>\*</sup>, Divya Kaur<sup>\*,‡</sup>, Van A. Ngo<sup>§</sup>, Xiuhong Cai<sup>\*,†</sup>, Junjun Mao<sup>¶</sup>, Umesh Khaniya<sup>\*,†</sup>, Xuyu Zhu<sup>\*,†</sup>, Sergei Noskov<sup>||</sup>, Themis Lazaridis<sup>‡,\*\*\*</sup> and M. R. Gunner<sup>\*,†,††</sup>

<sup>\*</sup>Department of Physics, City College of New York, City University of New York, New York, NY 10031, USA

<sup>†</sup>Department of Physics, The Graduate Center, City University of New York, New York, NY 10016, USA

<sup>‡</sup>Department of Chemistry, The Graduate Center, City University of New York, New York, NY 10016, USA

<sup>§</sup>Center for Nonlinear Studies, Los Alamos National Laboratory, Los Alamos, NM 87544, USA

<sup>¶</sup>Levich Institute, School of Engineering, City College of New York, City University of New York, New York, NY 10031, USA

<sup>||</sup>Department of Biological Sciences, Centre for Molecular Simulation, University of Calgary, Calgary, AB, Canada

<sup>\*\*\*</sup>Department of Chemistry, City College of New York, City University of New York, New York, NY 10031, USA

<sup>††</sup>Corresponding author. Email: [mgunner@ccny.cuny.edu](mailto:mgunner@ccny.cuny.edu)

**ABSTRACT:** Water molecules play a key role in all biochemical processes. They help define the shape of proteins, and they are reactant or product in many reactions and are released as ligands are bound. They facilitate the transfer of protons through transmembrane proton channel, pump and transporter proteins. Continuum electrostatics (CE) force fields used by program Multiconformation CE (MCCE) capture electrostatic interactions in biomolecules with an implicit solvent, which captures the averaged solvent water equilibrium properties. Hybrid CE methods can use explicit water molecules within the protein surrounded by implicit solvent. These hybrid methods permit the study of explicit hydrogen bond networks within the protein and allow analysis of processes such as proton transfer reactions. Yet hybrid CE methods have not been rigorously tested. Here, we present an explicit treatment of water molecules in the Gramicidin A (gA) channel using MCCE and compare the resulting distributions of water molecules and key hydration features against those obtained with explicit solvent Molecular Dynamics (MD) simulations with the nonpolarizable CHARMM36 and polarizable Drude force fields. CHARMM36 leads to an aligned water wire in the channel characterized by a large absolute net water dipole moment; the MCCE and Drude analysis lead to a small net dipole moment as the water molecules change orientation within the channel. The correct orientation is not as yet known, so these calculations identify an open question.

**KEYWORDS:** Water simulation; molecular dynamics; Monte Carlo; polarized force field.

### 1. INTRODUCTION

Water is a unique solvent, with a high dielectric constant and a facile ability to make hydrogen bonds. It plays an important role in determining the structure and cellular localization as well as the dynamics, and function of proteins and other biomolecules.<sup>1</sup> It is the solvent for biochemical reactions as well as the substrate or product in many reactions. Water drives the formation of membrane bilayers and of properly folded proteins by solvating charged groups on the surface,

while favorable water–water interactions lead to the burial of hydrophobic moieties.<sup>2</sup> Stabilization of charged groups by water modulates the proton affinity of acidic and basic side chains and ligands. Its high dielectric constant screens long-range electrostatic interactions.<sup>3</sup> The release of water molecules from apo-protein cavities can have significant effects on ligand

Received: 24 January 2020

Accepted: 16 April 2020

Published: 4 July 2020

binding selectivity and affinity.<sup>4</sup> Water is a weak acid and base, so leads to a low concentrations of solvated hydronium and hydroxyl ions in neutral, aqueous solutions.

Protons play key roles in cellular reactions.  $H^+$  is often a biochemical reactant. Protons transfer into buried active sites or through membrane embedded proton pumps, such as bacteriorhodopsin<sup>5</sup> and the heme-copper oxidases.<sup>6,7</sup> The transmembrane pH gradient, is a vital store of cellular energy. Protons are transferred via water molecules or polar side chains.<sup>8,9</sup> While we will refer to the mobile proton, a proton is always associated with one or more water molecules. Hydronium is a minimum unit, but the proton is more likely to be associated with two water molecules as a Zundel cation or as a larger, Eigen complex. Water associated protons move through proton specific channels<sup>10–13</sup> and play a role in proton dependent ion and substrate transporters.<sup>14,15</sup> Transiently hydrated cavities help control the connectivity of proton pathways between the two sides of the membrane.<sup>5–7</sup> Naturally occurring short peptide antibiotics, such as gramicidin work by forming open channels allowing protons and other cations to pass through the targeted cell membrane, dissipating essential gradients.<sup>16,17</sup>

Water molecules in oriented water wires with aligned dipoles facilitate proton transfer via the Grotthuss mechanism.<sup>18–20</sup> The water wire starts with dipoles oriented in one direction and ends facing the opposite direction. The water wire then must flip back to the original dipole direction to prepare for the next proton transfer.<sup>21–23</sup>

The stability of an aligned water wire and the barrier to reorientation is likely to depend crucially on the local dielectric environment of the narrow channel. Classical MD simulations with additive force fields have been used to study the dynamics of water molecules confined in ion channels.<sup>21,24,25</sup> The classical force fields such as AMBER or CHARMM36 assign fixed partial charges to all atoms, fixing the water molecule dipole moment. However, the complex chemistry of permeation pathways presented by narrow pores such as the gramicidin A (gA) channel should lead to a significant, dynamic, induced component of the water molecular dipole moment.<sup>26–30</sup> The importance of induced polarizability for water molecules has been shown in various systems such as the stability and dynamics of individual hydrogen-bonds<sup>31–33</sup> as well as of water molecule binding to the surface of nanomolecule or proteins.<sup>34–36</sup> Polarizability may thus affect potential barriers and ion transport properties across the narrow channels.<sup>30,37</sup> Therefore, an account of the induced

dipole component of water molecule interactions are critical to assess the accuracy of models as they try to account for the thermodynamics of proton-induced wire reorganization in proteins. A detailed understanding of the role of water molecules confined in the narrow pores and the inter-play between the solvent-protein and solvent-ion interactions can help provide more clues for accurate descriptions of proton transport in gA and other channels.

gA is a model system that has long been used to study water molecules, protons and ions in channels.<sup>12,30,37,38</sup> gA consists of 15 alternating l- and d-amino acid residues in two right-handed  $\beta$ -helices, with the N-terminus of both helices meeting in the center of the membrane. The N-terminus is capped with a formyl group and the C-terminus with an ethanolamine. The  $\beta$ -helical structure has side chains pointing away from the channel pore, leaving sufficient space for water molecules to form a single-file water wire within the channel.<sup>39</sup> gA is a simple model system, with few conformational degrees of freedom and no protonatable residues. Thus, the balance of water:water, water:protein and water:ion interactions can be dissected (relatively) cleanly. Various computational methods have been used to study the protein stability,<sup>40,41</sup> as well as the water, proton and ion conductions and selectivity.<sup>38,42</sup> Implicit and explicit water models have been used<sup>43</sup> with nonpolarizable<sup>40</sup> and polarizable<sup>30</sup> MD force fields. MD analysis has been compared with experimentally determined barriers and rates for conductance of ions and protons.<sup>17</sup>

gA provides an ideal, simple model system to directly compare the properties of water molecules confined in a protein found by different simulation techniques and levels of theory. The presence of a single-file water wire in gA is well established and its dynamical reorganization is known to play a significant role in monovalent cation and proton permeation. The work presented here briefly reviews methods to treat water molecules in molecular simulations then compares the behavior of water wires in the gA channel obtained with classical MD trajectories, trajectories using the Drude polarizable force field and the Multi-conformation Continuum Electrostatics (MCCE) program which is a Continuum Electrostatics/Monte Carlo (CE/MC) method. MCCE simulations are run on snapshots from the classical MD trajectory. The MD simulations use explicit water molecules inside and outside of the channel. The MCCE calculations monitors explicit individual water molecules within the channel with an implicit, continuum solvent outside of the membrane embedded protein. The resulting

average number of water molecules in the channel, and the water dipole orientation are compared for different methods. The different methods give surprisingly different results. The dipole moment of water confined in gA can be used as a reporter of the net alignment of the water molecules. In the classical MD trajectories obtained with the CHARMM36 force field, the water molecules are highly aligned through the whole permeation pathway. They change direction quickly with rare turns. In contrast, the dipole moment for water modeled with the Drude polarizable force field has the peak in the average dipole moment near zero showing they are not aligned through the channel and the orientation changes often through the trajectory. In MC simulations with TIP3P water parameters and CE energies, water molecules in the channel also have a small summed dipole moment. Increasing the size of the water atomic charges in MCCE results in a dipole distribution closer to that found in the classical MD force field with an aligned water wire. MCCE is used to calculate the barrier for proton transfer through the gA channel, which is found to be in good agreement with the results of earlier empirical valence bond (EVB) calculations.<sup>44</sup>

### 1.1. Explicit water molecules

Water molecules are challenging to include in molecular simulations. They are present at a concentration of  $\approx 55.5$  M so many individual molecules are required to reproduce the solvent properties. The charge distribution is only approximated by standard fixed charge force fields since the electron distribution is polarized by the local environment.<sup>45</sup> The parameters for water molecules in MD simulations can use fixed charge force fields<sup>46</sup> or polarizable descriptions of the charge.<sup>27,47,48</sup> The dielectric constant of water is time-dependent, starting with the optical dielectric constant of 2 on the picosecond time scale, then taking picoseconds to nanoseconds to relax to its static value near 80.<sup>49,50</sup> The time for dielectric relaxation provides an estimation of how long calculations with explicit water molecules need to bring the water to equilibrium in an MD simulation. Water molecule force fields remain a continuing focus of innovation and modification.<sup>51–59</sup>

### 1.2. Properties of water modeled with implicit solvent

Water molecules can also be included in simulations by averaging their behavior with implicit models of

solvent water.<sup>3</sup> This method aims to reproduce the equilibrated electrostatic dielectric properties of water, including ionic strength dependent solvation and screening of ions, as well as the contribution of surface area dependent hydrophobic energy and attractive Lennard–Jones interactions.<sup>60</sup> CE provides the foundation for implicit solvent analysis. For MC calculations, the electrostatic potential is often determined by the Poisson–Boltzmann equation of CE.<sup>3</sup> In MD simulations, the Generalized Born implementation is often used.<sup>61</sup> Implicit solvent methods have strengths and weaknesses when compared to those that use explicit water molecules.<sup>62</sup> Implicit solvent is always at equilibrium with the charges in the system, so greatly reduces the burden of sampling water molecule configurations.<sup>62</sup> However, implicit water loses all information about individual water molecule dynamics, localization and orientation. In contrast, explicit water captures the motion of individual water molecule at the expense of requiring sampling and equilibrating the water molecules around the molecule of interest for tens of nanoseconds.

### 1.3. Molecular dynamics or Monte Carlo sampling

In addition to the choice of force fields to describe the system, molecular modeling relies on the method of sampling the available degrees of freedom. Molecular dynamics (MD) moves atoms following Newton's laws of motion given the forces generated by the force fields at the time-dependent atomic positions. Monte Carlo (MC) sampling is an alternative approach to generate a Boltzmann ensemble of microstates of molecules.<sup>63</sup> MC has advantages and disadvantages when compared to MD methods. While MD generates moves from knowledge of local forces, MC moves are random, with their acceptance controlled by the system free energy. The goal is to achieve an equilibrium ensemble of individual states of the molecule of interest, losing information about the pathway or rates of processes. If equilibrium is achieved thermodynamic analysis can be straightforward in MC simulations as the energies of all microstates in the equilibrated ensemble are known.<sup>64</sup> MC moves can change atomic positions of the macromolecule, the distribution of bound and free ligand. In addition, MC can sample different chemical states of the system.

A group of MC methods have been developed for accurate calculation of the  $pK_a$  and redox midpoints,  $E_m$ s, of residues and ligands in proteins.<sup>3,65</sup> Changing

protonation states represents a chemical reaction so cannot be treated by standard MD analysis, although constant pH<sup>66–68</sup> or  $E_h$ .<sup>69</sup> MD techniques are being developed to handle these processes. MC methods is often combined with a CE force field to calculate electrostatic energies.<sup>70,71</sup> These CE/MC methods have the advantage of providing accurate electrostatic energies, taking into account electronic polarization with a dielectric constant of 2 that is missing in classical nonpolarizable MD, which uses a dielectric constant of 1.<sup>72</sup> Higher dielectric constants for the protein are used to model protein flexibility.<sup>73,74</sup> These CE/MC methods generate ensembles of protonation or redox states following changes in proton chemical potential (i.e. the pH).<sup>3</sup> Ligand binding has been treated by Grand canonical MC (GCMC), measuring the affinity of explicit ions<sup>75,76</sup> or hydronium<sup>77</sup> binding to proteins in implicit solvent water. MD simulations follow the position changes of atoms over time in an unchanging chemical state and thus fix the protonation states of all residues. GCMC sampling thus allows ionization state changes which conventional MD simulations do not.<sup>78</sup>

### 1.3.1. Degrees of freedom in the MCCE program

The MCCE is the CE/MC program that will be used here. It retains a rigid protein backbone, but allows full rotamer side chain search.<sup>79</sup> It also allows GCMC sampling of binding of explicit water, ions<sup>80</sup> and other small ligands to access relative binding affinities.<sup>81</sup> One microstate is made up of one choice of position and protonation states for each side chain, ligand and associated explicit water. The choice for each group is called a conformer. The energy of each state is the sum of interactions with the continuum solvent (solvation energy) and pairwise interactions calculated with the rigid backbone and amongst all side chain and ligand conformers in that microstate. The final result is the probability of choosing each conformer of each residue in the Boltzmann distribution. Changing the ligand chemical potential or pH changes the equilibrium distributions so gives the binding affinity of ligands and the  $pK_a$  of acids and bases.

## 1.4. Use of Monte Carlo sampling with explicit water

In most CE/MC applications, water molecules are removed from the simulation and replaced by an implicit solvent with a dielectric constant of 80. Hybrid CE/MC methods use MC sampling, with a CE force field, with implicit solvent outside of the macromolecule, while

explicit water molecules with many conformational choices are available for sampling within cavities. Calculations comparing the  $pK_a$ s of residues deeply buried within bacteriorhodopsin using only implicit solvent with those using explicit water molecules near key residues showed remarkably similar values.<sup>79</sup> Explicit water molecules have been used to follow proton pathways in proteins via MC sampling within CE/MC simulations.<sup>7</sup>

## 1.5. Modeling proton transfer in molecular dynamics simulations

Because proton transfer involves making and breaking of covalent bonds, it cannot be treated with classical MD simulations. Quantum mechanical methods, such as Car-Parrinello *ab initio* MD,<sup>82</sup> have offered important insights but at a substantial computational cost. Semiempirical methods based on valence bond theory<sup>83</sup> are much more efficient and have been used widely on a variety of problems.<sup>84,85</sup> Dissociative models that view water as a collection of free H and O particles have also been proposed,<sup>86–91</sup> but have so far been applied mostly to pure water or material science problems. The constant pH approach for modeling proton transfer combines classical MD simulation with periodic MC steps that move a proton to an eligible neighboring site.<sup>12,92</sup> However, the existing approaches violate detailed balance.<sup>93</sup> A method based on  $\lambda$ -dynamics<sup>94</sup> has also been proposed<sup>95,93</sup> but so far has been applied only to proton transfer between water molecules.

## 1.6. The barrier for hydronium transfer in Gramicidin channel

The proton gradient across energized bacterial, mitochondrial and chloroplast membranes provides the energy source for ATP synthesis and other processes. It is therefore necessary to control proton conduction without introduction of leaks.<sup>20</sup> gA collapses the proton gradient by poking a hole in the membrane. Protons are conducted through gA by the Grotthuss mechanism.<sup>20</sup> MD simulation,<sup>96,97</sup> umbrella sampling,<sup>96</sup> and multistate EVB (MS-EVB)<sup>98</sup> have been used to analyze the thermodynamic properties of the proton in channels leading to conduction. In this paper, MC sampling is used to calculate the energy of a hydronium molecule moving through the gA channel. The energy difference for a hydronium in water or in the gA channel is compared with that calculated using the EVB method.<sup>44</sup>

## 2. METHODS

### 2.1. gA protein model

The starting structure of the gA dimer was derived from the X-ray structure (PDB ID: 1JNO). Each of the gA monomers has the sequence: formyl-Val<sub>1</sub>-Gly<sub>2</sub>-Ala<sub>3</sub>-DLeu<sub>4</sub>-Ala<sub>5</sub>-DVal<sub>6</sub>-Val<sub>7</sub>-DVal<sub>8</sub>-Trp<sub>9</sub>-DLeu<sub>10</sub>-Trp<sub>11</sub>-DLeu<sub>12</sub>-Trp<sub>13</sub>-DLeu<sub>14</sub>-Trp<sub>15</sub>-ethanolamine. The two monomers are each oriented with their N-terminus in the middle of the membrane.

### 2.2. Classical MD simulations

The simulation protocol was generated within the CHARMM-GUI, based on optimal settings for simulations of protein-membrane systems in OpenMM.<sup>99</sup> The parameters for the N- and C-termini formyl and ethanolamine caps for both classical MD and MCCE are taken from Ref. 12. For Classical MD simulations, the protein was embedded in a 1,2-dimyristoyl-sn-glycero-3-phosphocholine (DMPC) membrane using the CHARMM-GUI Web server.<sup>99</sup> The CHARMM36 force field is used for the protein and lipids and TIP3P model is used for water molecules. This puts a charge of  $-0.834$  on each water oxygen.

An initial energy minimization is carried out for 500 steps with heavy atoms of the protein and lipid molecules restrained with a force constant 4000, 2000 and 1000 kJ/mol/nm<sup>2</sup>, for protein backbone, side chain and lipid heavy atoms respectively. A step-wise equilibration was performed in the NPT ensemble, where restraints on the heavy atoms are gradually released. The pressure was regulated by MC membrane barostat in OpenMM at a pressure of 1 bar and a pressure coupling frequency of 100 simulation steps. The temperature was maintained at 303.15 K using Langevin thermostat. The simulations were carried out using OpenMM (GPU version).<sup>100</sup> Snapshots were saved every 1 ps for 200 ns. The restrained MD trajectories were carried out with the channel restrained with a positional restraint force 50 kJ/mol/nm<sup>2</sup> for the gA backbone.

### 2.3. MD simulations with Drude force field

The 2013b version of CHARMM Drude force field for proteins and lipids was used.<sup>101–104</sup> The parameters for ethanolamine and formyl groups present in gA were taken from Ref. 105. The SWM4-NDP model is used for water molecules in the channel and in bulk.<sup>101</sup> It consists of two hydrogens (with charge 0.557330),

one oxygen (with charge  $-1.11466$ ). Charged auxiliary particles are attached to the oxygen with springs.

The equilibrated system from Refs. 28 and 101 was used to generate the starting configurations for MD simulations with the Drude polarizable force field. The resulting simulation systems contained the gA channel embedded into a lipid bilayer comprised of 96 DMPC molecules solvated by 4003 SWM4-NDP water.<sup>28,101</sup> A hexagonal periodic cell with a side of 61 Å and length of 77 Å was used for all production simulations. Langevin dynamics with a dual-thermostat scheme was used to propagate the atoms and auxiliary Drude particles with an extended Lagrangian formalism implemented in the NAMD package.<sup>102,106</sup> The thermostat acting on heavy (non-Drude) particles was set to  $T_{\text{heavy}} = 330$  K to enhance sampling of lipid dynamics as suggested previously.<sup>107</sup> The Langevin damping coefficient was set to 1.0 ps<sup>-1</sup>. The weak damping coefficient enables stable Drude production runs with an integration time step of 1.0 fs.<sup>108</sup> For all production runs,  $T_{\text{Drude}} = 0.1$  K was used with a spring constant for the atom-Drude bond of 1000 kcal/mol/Å<sup>2</sup>.<sup>109,110</sup> A damping constant of 20.0 ps<sup>-1</sup> was applied to Drude particles.

### 2.4. MCCE simulations

MCCE is used to carry out the CE/MC simulations of the water molecules in the gA channel.<sup>79</sup> In MCCE a conformer is a specified set of positions and charges that can be chosen in MC sampling for the residue or ligand. These provide the degrees of freedom for a protein with a fixed backbone. Conformers are made prior to MC sampling and all energy terms are pre-calculated. Microstates, which specify the conformer for each residue and ligand, are subjected to GCMC sampling.<sup>78</sup>

The energy of a microstate includes self-energy electrostatic solvation energy and torsion energy for each conformer, which are independent of the choices for other residues. To these are added the pair-wise Lennard-Jones and electrostatic interactions between all conformers in the microstate. For GCMC binding calculations as carried out here, the water molecules chemical potential is considered.<sup>81</sup> For pH titrations, the free energy of group ionization at the pH of the calculation is included.<sup>111</sup> Thus, the free energy cost of producing a hydronium in solution is a component of the calculation of the free energy of hydronium transfer through the channel.

Electrostatic interactions are calculated with DelPhi<sup>112</sup> using PARSE charges and radii<sup>113</sup> with a

dielectric constant of 4 for protein and featureless slab which mimics the membrane and 80 for water with 150 mM implicit ions.<sup>78</sup> Amber non-electrostatic parameters are used.<sup>114</sup> As with the classical MD simulations the N- and C-termini formyl and ethanolamine caps are taken from earlier calculations<sup>12</sup> and the default water model is TIP3P with the partial charges of O:  $-0.834$  and H:  $0.417$ . The standard MCCE calculations were carried out at 298 K. Additional simulations are presented where the temperature was raised to 330 K for Metropolis sampling and the dielectric constant for water was reduced to 70. The internal dielectric constant remained at 4.

## 2.5. Placing explicit water molecules in the channel in MCCE

Each MCCE calculation starts with a snapshot from the backbone restrained classical MD trajectory with all water molecules and lipids removed. As used for the MCCE simulations of other membrane proteins the protein is embedded in a  $35 \text{ \AA}$  tall low dielectric slab using the Implement Protein Environment for CE (IPECE) utility.<sup>79</sup> This is a minimal, implicit membrane model, whose sole purpose is to form a region with a low dielectric constant around a protein.

Protein coordinates are taken from nine snapshots of the MD restrained trajectory. These are chosen based on the summed dipole moment of the water molecules in that snapshot. Thus, the water molecules in three of the snapshots have a net positive dipole moment, three have a negative dipole moment and three have summed dipole moments near zero. The results presented for the MCCE calculation are the sum of the results starting with each snapshot, weighted by probability of each dipole moment in the trajectory.

Water molecules were added to the channel on a  $7 \text{ \AA} \times 7 \text{ \AA} \times 22 \text{ \AA}$  rectangular grid with  $0.5 \text{ \AA}$  spacing oriented along the channel  $z$ -axis. Grid points that clash with the protein atoms were removed. An oxygen atom was placed at the approximately 700 remaining grid points. For each oxygen, a fixed number of water molecule conformers were generated by applying 10 random rotations to place protons on the fixed oxygen position (Fig. SI.1). Thus,  $\approx 7000$  water molecule conformers are sampled. A comparison analysis considering 5, 10, 15, or 20 different proton positions (water conformers) is shown in Fig. SI.2. The default calculations included 10 water conformers/oxygen.

## 2.6. Tests for convergence of the water molecules in the gA channel in MC sampling

In MCCE we evaluated convergence in two ways. One is the stability of measurable outcomes, these being the distribution of the number of water molecules in the channel, the number of hydrogen bonds and the summed dipole moment of these water molecules. The more rigorous test is the difference in the Boltzmann averaged energy for 100 restarts of MC sampling. With the TIP3P water charges the full width at half maximum (FWHM) of the average energy distribution is generally  $\approx 0.2\text{--}0.3 \text{ kcal/mol}$  and all MC restarts have an average total energy range within  $\approx 0.4 \text{ kcal/mol}$  (Fig. SI.3). Microstates created in different input snapshots do have different energy resulting from the differences in the input protein backbone and side chain conformation.

Three methods are used to enhance convergence. (1) The oxygens are grouped so that all water conformers, where the oxygen has the same  $z$ -coordinate, are treated as one residue, so that only one conformer from the slice can contribute to a given microstate. All water molecules in one layer are too close to each other so they can never be present in the same accepted microstate. Thus, grouping them in one residue eliminates the chance that any microstate with two water molecules in the same layer would be evaluated as a proposed microstate and then rejected. There are 44 layers, separated by  $0.5 \text{ \AA}$ . (2) The ratio of conformers in the channel and outside in the bulk is varied. There are  $\approx 7000$  conformers to choose from but only approximately 7 will be in the channel at one time. Each layer has  $\approx 10$  oxygens and thus 100 different choices for water molecule conformers in the gA channel. Six to ten chances to move out of the protein are included for each layer. Water molecules transferred to the bulk have an electrostatic solvation (reaction field) energy of  $-2.6 \text{ kcal/mol}$ , which is the value calculated for a TIP3P water molecule in solvent with a dielectric constant of 4 inside and 80 outside. (3) The number of new conformer choices made for each microstate helps to reduce the memory of the system. Standard MCCE makes from 1 to 3 changes before evaluating the energy. Here 10 to 20 changes are applied before calculating the energy of the new microstate and applying Metropolis criteria for acceptance.

The calculations with TIP3P water atomic charges are well converged, giving both consistent averaged microstate energy and physical properties. We will present some information about MCCE calculations

with a larger water partial charge on the water molecule that can reproduce elements of the behavior of the classical MD trajectories. For larger charge of water model, the measurable properties we present are robust, but the energy difference between multiple restarts of MC sampling have significantly different energies. Thus, while the large charge calculations provide useful information, they are very difficult to converge.

## 2.7. Water chemical potential

We have not set out to independently calculate the absolute binding affinity of the ligand water molecule in the MCCE simulations. Rather energy is added to the ligand solution chemical potential in a binding titration to match experimental or other computational results. In previous studies of ion binding, an experimental  $K_d$  is used to define the concentration at a given MCCE energy.<sup>80</sup> Here, we will compare the distribution of the number of water molecules in the channel in MCCE and in the MD calculations.

In MCCE, it is recognized that the ratio of available reactant to product conformers changes the outcome. A correction for this imbalance, which excludes the conformers that are at high energy and so are never in accepted microstates need not be considered, is included in the standard MCCE program.<sup>78</sup>

## 2.8. Analysis of the water molecules in the gA channel

When carrying out calculations using different force fields it is difficult to directly compare energy terms. In addition, as the different methods have different degrees of freedom, contribution of entropy to the results will be different. A Solvation Structure and Thermodynamic Mapping (SSTmap)<sup>115</sup> analysis of the classical MD trajectories and an analogous analysis of energy terms in MCCE for water molecules are found in Table SI.2. In the main text, we will focus on observable water properties in the channels where the outcome of the different calculations can be directly compared.

### 2.8.1. Counting water molecules

The number of water molecules in the channel is a function of the relative energy of the water in bulk solvent and in the channel. For the MD simulation, the total number of water molecules inside the gA channel is determined using VMD.<sup>116</sup> Frames separated by 20 ps are aligned with each other along the  $z$ -axis, the root-mean-square deviation (RMSD) of atomic

positions of 200 ns restrained and unrestrained structures are shown in Fig. SI.4.

The water molecules where the oxygen coordinates are within the limits of the gA channel protein are considered inside the channel. In the MCCE simulation, explicit water molecule conformers are only placed within the channel. The water molecules count is the average number of explicit water molecules bound in the GCMC accepted microstates.

### 2.8.2. Dipole orientation

The dipole moment describes the overall orientation of water molecules in the gA channel in a given MD snapshot or MC microstate. The channel is aligned along the  $z$ -axis, through the membrane. The  $z$ -component of the dipole moment is given by

$$\mu_z = q_0 * r_z, \quad (1)$$

where  $q_0$  is the charge on the oxygen and  $r_z$  is the vector sum of the  $z$ -components for each O–H bond. The dipole moment is determined individually for each MD snapshot or MC microstate as the sum of  $\mu_z$  for each water molecule in the channel.

The Dipole Moment Watcher tool in VMD is used to calculate the dipole moment for every frame in the MD trajectory. For the Drude MD trajectory, only the real atoms are considered, the oscillator positions are not included. For MCCE simulation the dipole moment is calculated independently for the water molecules in each accepted microstate. A histogram of the dipole moments for each set of conditions used a standard bin of 0.1 D. The  $z$ -component of the dipole moment of the gA protein backbone in each frame of the classical MD trajectory is also calculated with the VMD tool (Fig. SI.5).

### 2.8.3. Count of hydrogen bonds between water molecules and from water molecules to protein backbone

Hydrogen bonds made between neighboring water molecules  $N_{ww}^{\text{HB}}$  or between a water molecule and the protein backbone  $N_{pw}^{\text{HB}}$  are counted if the distance between heavy atoms is  $\leq 3.5 \text{ \AA}$  and hydrogen–donor–acceptor angle is  $\leq 30^\circ$ .

## 3. RESULTS AND DISCUSSION

### 3.1. Number of water molecules within the gA channel

The number of water molecules in the gA channel at equilibrium is a function of both the free energy of the

**Table 1.** Average number of water molecules in gA channel.

Simulation methods	Water charges	Water count
CHARMM36 (restrained)	O: $-0.834$ , H: $0.417$	$7.84 \pm 0.93$
CHARMM36 (unrestrained)	O: $-0.834$ , H: $0.417$	$7.38 \pm 0.95$
Drude	O: $-1.114$ , H: $0.557$	$5.93 \pm 1.09$
MCCE_303K	O: $-0.834$ , H: $0.417$	$7.37 \pm 0.19$
MCCE_330K	O: $-0.834$ , H: $0.417$	$7.35 \pm 0.18$

Note: The classical MD trajectories were carried out at 303.15 K.

water molecules in bulk solvent and their energy in the channel. Explicit water MD simulations are carried out using the standard CHARMM36 force field as well as with the polarizable Drude oscillators. Table 1 shows the average number of water molecules in the channel and Fig. 1 shows the distribution of the count of the number of water molecules in individual MD snapshots or MC microstates. The 200 ns restrained MD trajectory has a narrow distribution, strongly favoring eight water molecules. The 200 ns unrestrained classical MD trajectory prefers seven water molecules in the channel. Previous experiment results also showed around seven water molecules inside the gA channel.<sup>117</sup> The MD simulation with the Drude force fields has on average

only six water molecules and has a wider range of water molecule numbers in the channel.

With the standard MCCE force field and added chemical potential of zero and no correction for the implicit water van der Waals interaction, the channel occupancy in MCCE is close to that seen with the unrestrained MD simulations. This may reflect the PARSE charge and radii used for the solution of the Poisson–Boltzmann equation in the calculation were optimized to replicate solute transfer data so these parameters model the energy of water molecule transfer without significant correction needed.<sup>118</sup> There are only modest differences in the distribution of water molecules in the gA channel for MCCE calculations initiated with different MD snapshots (Fig. SI.6).

The water chemical potential was modified for a single snapshot in MCCE to examine the binding isotherm Fig. 2. The channel saturates at approximately 14 water molecules, however after there are  $\approx 8$  water molecules the binding becomes somewhat anti-cooperative. Convergence of the MC sampling is evaluated by the distribution of the Boltzmann averaged energy for 100 independent MC runs. As the channel becomes more packed it becomes more difficult for the MC sampling to converge as the behavior of all water molecules become increasingly interdependent Fig. SI.7.

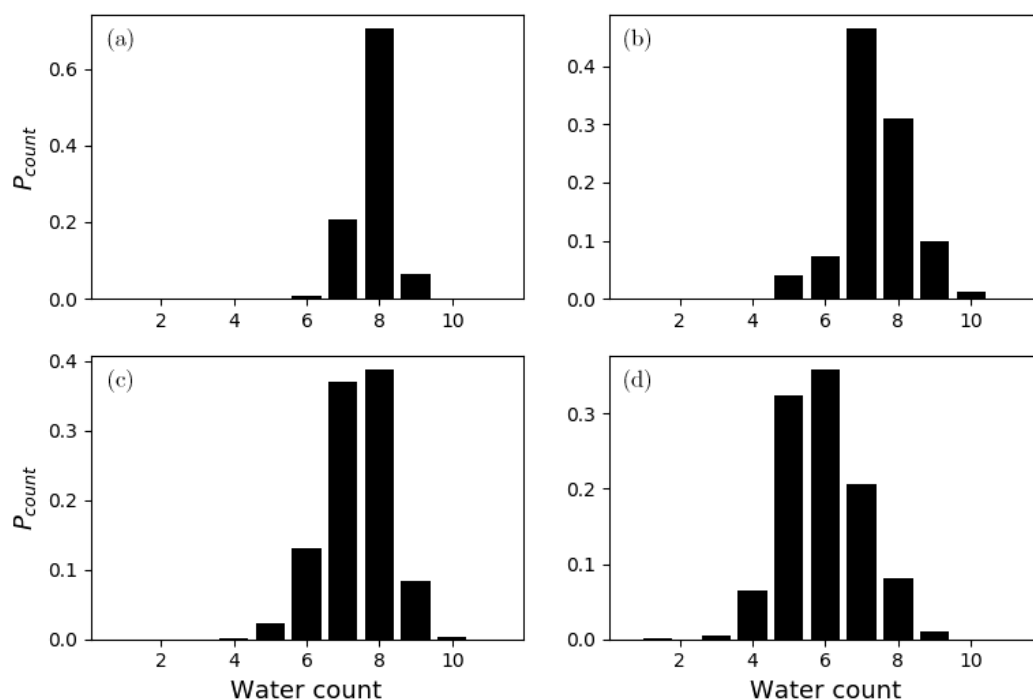


**Fig. 1.** Distribution of the number of water molecules inside the gA channel found in: (a) restrained MD trajectory with CHARMM36 force field; (b) unrestrained MD trajectory with CHARMM36 force field; (c) MC sampling using MCCE with TIP3P charges; and (d) MD trajectory with Drude force field.

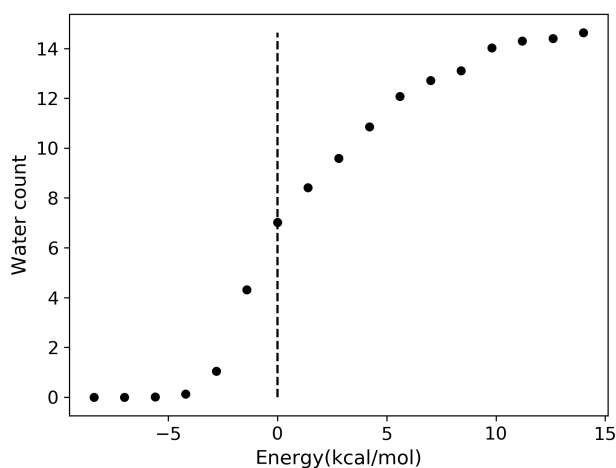


**Fig. 2.** Average number of water molecules in the gA channel as a function of the extra, unfavorable chemical potential added to water molecules in bulk solvent in the GCMC simulation in MCCE. All other calculations reported here have zero energy added to bulk water chemical potential.

## 3.2. Dipole orientation of water molecules inside gA channel

### 3.2.1. MD simulation

The gA protein is made up of 2 identical  $\beta$ -helices each 15 amino acids long,<sup>16</sup> oriented so the two N-termini meet in the middle of the membrane. The N- and C-termini are capped with the neutral formyl and

ethanolamine groups, respectively, so there is not charge on the termini. The  $\beta$ -helix alternates the orientation of adjacent amides (as in a  $\beta$ -strand) so it does not build up a helix macro-dipole as would be found in an  $\alpha$ -helix. The summed amide dipole moment of the backbone along the membrane  $z$ -axis,  $\mu_{z,\text{prot}}$  is close to 0 (Fig. SI.5). The question then is whether the water molecules inside the gA channel align with the helix, flipping in the middle, or if the water:water interactions ensure that they keep one orientation through the channel. The three computational methods find different equilibrium water orientations.

The dipole moment of the water molecules in the channel was calculated along a 200 ns restrained, classical MD trajectory. (Fig. 3(a)) A histogram of the summed water dipole moments ( $\mu_{z,\text{wat}}$ ) show two clear peaks at  $\pm 14$  Debye (Fig. 3(a)) with a FWHM of  $\approx 3$  D as has been found previously.<sup>119</sup> The sign of the orientation is arbitrary but is used consistently for a given trajectory. Typical water molecule positions in states with positive, negative and near 0 Debye dipole moment are shown in Fig. 4. After 200 ns, the probability 45.5% of the snapshots have water molecules oriented in the positive direction, 1.1% have a dipole moment near zero (+5 Debye to  $-5$  Debye), while 53.4% are oriented in the negative direction. The flips between positive and negative orientation are rare. Thus, these

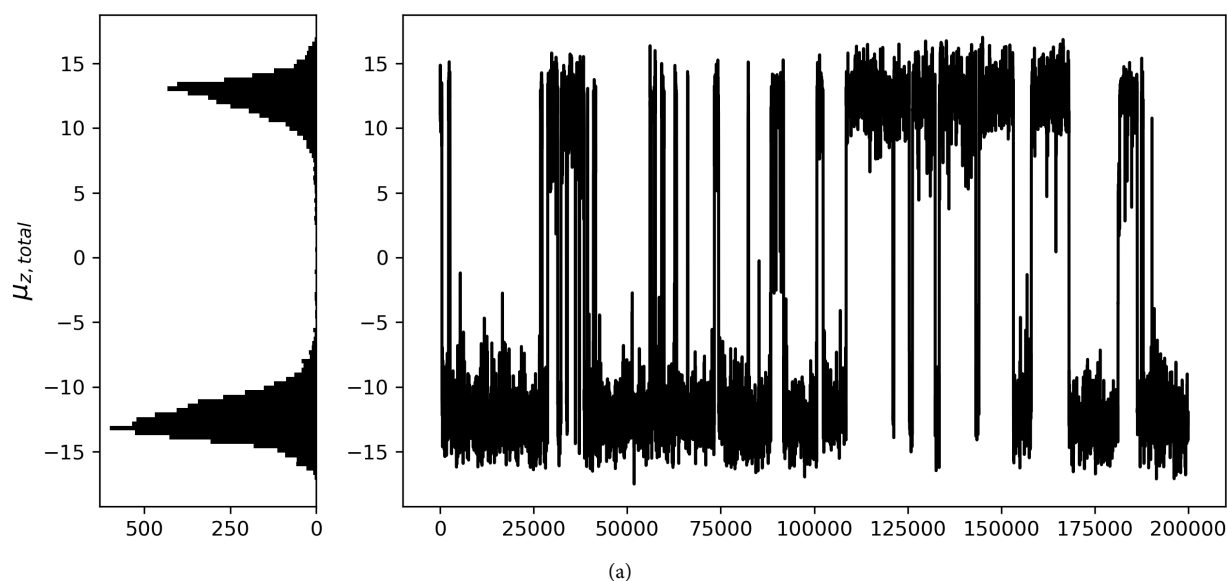


**Fig. 3.** Summed dipole moment for the water molecules in the gA channel in each snapshot in the MD trajectories. Left: The distribution of the water dipole moments. Right: The dipole moment of the water molecules inside the gA channel through each trajectory as a function of time. (a) Restrained MD trajectory with CHARMM36 force field; (b) unrestrained MD trajectory with CHARMM36 force field and (c) MD trajectory with Drude force field.

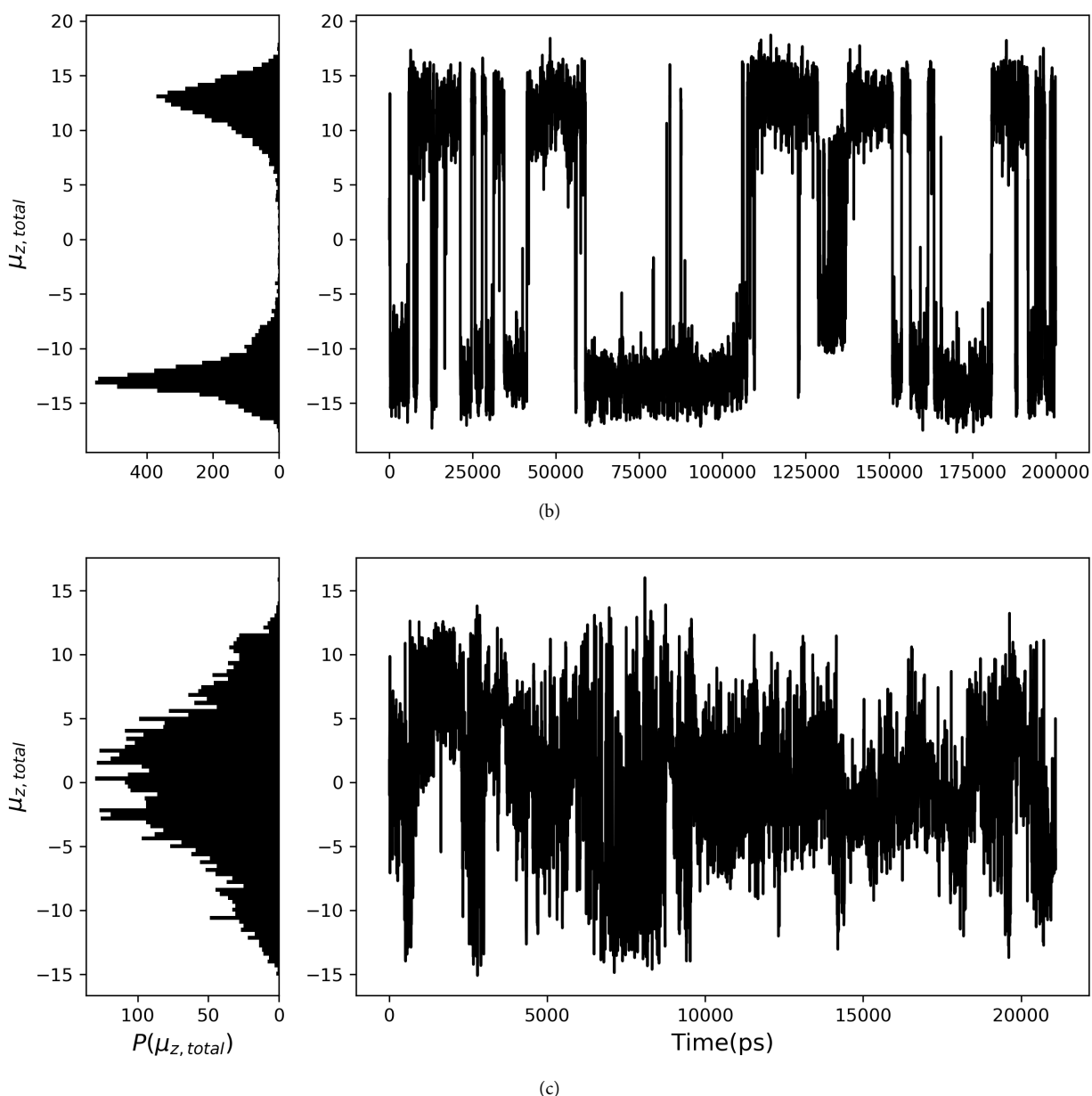


Fig. 3. (Continued)

water molecules maintain an ordered water wire that persists through the channel, rather than changing orientation in the middle of the channel. It should be noted there is no transmembrane potential nor ions in any of these simulations to orient the water molecules in the channel.

The transition between states with positive and negative dipole moments states of the water wire takes only  $\approx 6$  ps, starting at one end and zipping along to the other side (Fig. 5). This is the orientation change required for the Grotthuss mechanism.<sup>20,38</sup> With 97 flips/200 ns the flip rate is  $\approx 4.9 \times 10^8$  flips/s. The rate ( $k$ ) is  $k = k_0 \times 10^{-E_a/kT}$ . Using the standard value of

$k_0$  of  $\approx 10^{13}$ /s, the flip barrier is  $\approx 5.8$  kcal/mol. This estimate of the barrier obtained from the measured frequency of transition is higher than the 2–3 kcal/mol estimated previously from PMF simulations at 330 K. The trajectory here is run at 303.15 K, which may contribute to there being fewer flips.<sup>20,119</sup>

When the restraints on the amide backbone are released in the classical CHARMM36 MD trajectory the water wire remains oriented through the channel, with two peaks in the  $\mu_{z, wat}$  histogram near  $\pm 14$  Debye (Fig. 3(b)). The flip rate is  $\approx 3.25 \times 10^8$  flips/s. This suggests the barrier is  $\approx 6.0$  kcal/mol, similar to the value found with the restrained simulation. A running

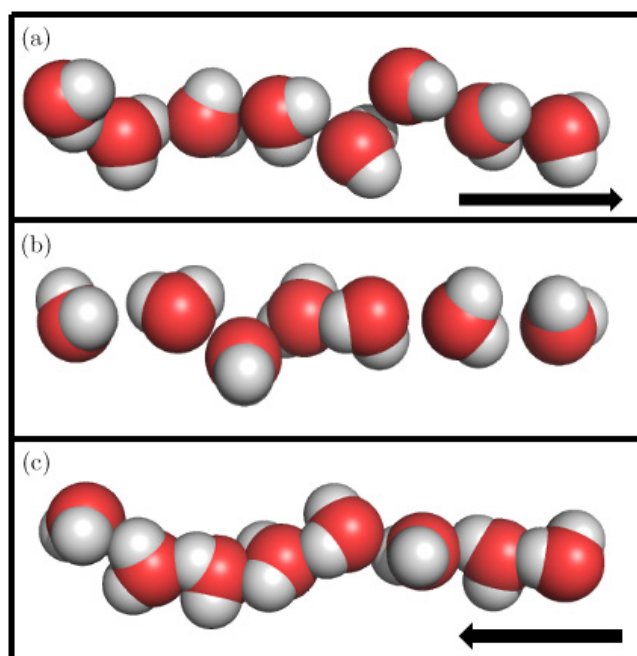


**Fig. 4.** Example of water orientation for the microstates with: (a) positive dipole moment; (b) near zero dipole moment and (c) negative dipole moment. Each figure represents one snapshot from the restrained MD trajectory.

sum of the averaged dipole moment with time shows that the dipole moment requires at least 150 ns to converge to an approximate 50:50 mix of positive and negative facing water wires (Fig. SI.8).<sup>20</sup> In contrast, the water wire orientation in the restrained MD trajectory converges in less than 50 ns. However, in all trajectories, the probability that the sum of the water dipole is near zero remains very low at  $\approx 1\%$ .

The behavior of the water molecules in the gA channel was explored with the Drude polarizable force field and SWM4-NDP water model. The results are quite different than found in the classical CHARMM36 MD simulations. The cumulative water dipole now has a broad distribution peaked between 0 D and  $\pm 4$  D (Fig. 3(c)). The water molecules are rarely fully oriented in either direction. In addition, the dipole orientation is very dynamic, changing often through the trajectory.

### 3.2.2. MC simulation

The total dipole moment of the water molecules inside the channel is determined for each microstate, where a microstate is analogous to a frame in an MD trajectory.

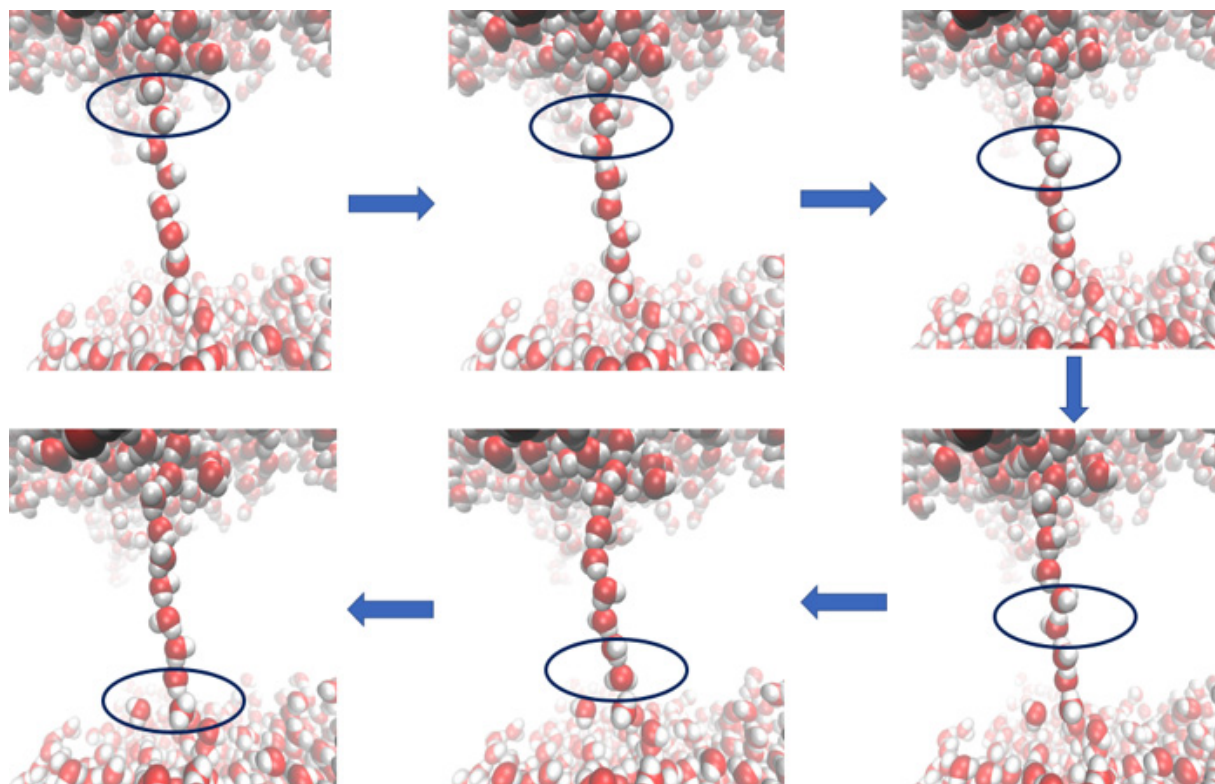


**Fig. 5.** Series of snapshots separated by 1 ps from in the restrained classical force field MD trajectory which shows the process by which the water wire in the gA channel changes direction. The reorientation takes approximately 6 ps.

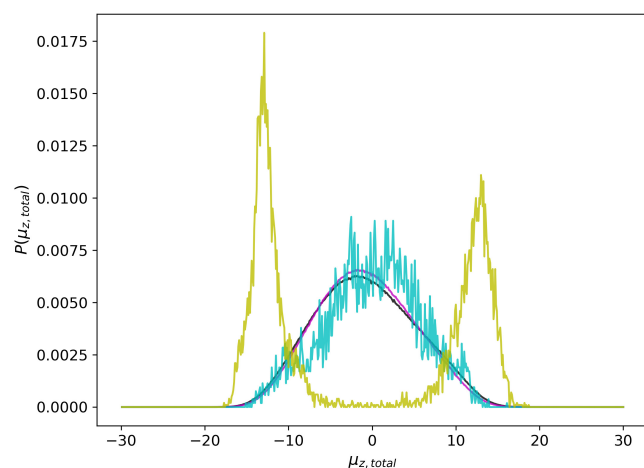


**Fig. 6.** (Color online) Comparison of the distribution of water molecule dipole moments in each MD snapshot or MC microstate. Water molecules in MCCE: Black line: 303.15 K; Purple line: 330 K. The dipole moment peak is slightly higher at the higher temperature. The results of MCCE simulations with TIP3P water, initiated with nine snapshots were, with three each for positive, negative and near zero net dipole moment and weighted by the probability of each dipole orientation in the MD trajectory (Fig. SI.9). Distribution of summed water molecule dipole moment in each frame of restrained CHARMM36 MD trajectory (yellow line) or Drude force field (cyan line) are reproduced from Figs. 3(a) and 3(c).

Here we have saved  $\approx 50$  million microstates for each independent MC sampling with the results from 100 independent MC runs added together for each snapshot.

The distribution of  $\mu_{z,\text{wat}}$  was determined. The single input MD snapshot has one water orientation with a unique dipole moment. However, MC sampling from any snapshot yields a broad distribution of dipole moments, which usually has a single peak (Fig. SI.9). Thus, while MCCE analysis of an individual MD snapshot cannot capture the full spread of the full MD trajectory, it does show a broad distribution of water orientations in the Boltzmann distribution of microstates that are acceptable in this protein.

The results were obtained using protein structures from the restrained MD snapshots with positive, negative or near zero dipole moment. The MCCE results from each snapshot were summed, weighted by the probability of these positions in the MD trajectory to generate the properly weighted dipole moment distribution (Fig. 6). The overall dipole moment distribution shows one broad peak centered near 0 Debye, more similar to that found with the Drude, polarizable force field than with the classical MD analysis. The dipole distribution is little changed when the temperature

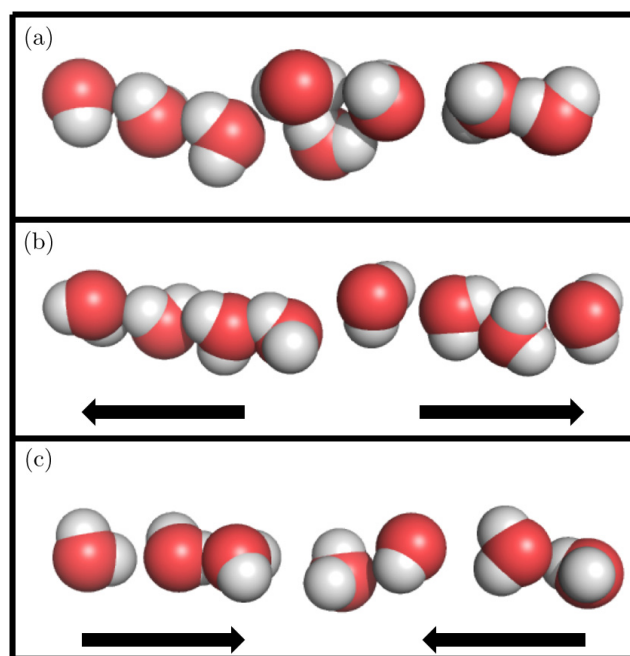


**Fig. 7.** Examples of water molecules in gA channel whose summed dipole moment is between  $\pm 1$  Debye: (a) water molecules are disordered; water molecules flip orientation in the middle; with protons oriented towards: (b) the outside of the channel and (c) the center of the channel.

for the Metropolis acceptance is carried out at 298 K or 330 K.

### 3.2.3. The orientation of the states with a net dipole moment near zero

In the dipole moment distribution from the MD trajectory with the Drude force field and in the MCCE simulation with TIP3P water model, there are many states which have a dipole moment near 0 Debye. There are two ways to get a summed dipole moment near zero. One is that the water molecules flip in the middle of the gA channel pointing their protons towards the NTR (or CTR). The other way is that they are disordered so are not orientated strongly to the protein or to each other (Fig. 7).

The dipole moment is calculated separately for water molecules inside the two helices. For the states with a net dipole between  $-1$  and  $1$  Debye, 30% of the snapshots in the Drude trajectory are disordered, while 20% of the microstates are disordered in the MCCE MC sampling (Fig. 7(a)). The rest are oriented, but reverse direction in the middle when the two peptides come together. In the Drude trajectory, approximately 35% the water molecules have their oxygens pointing towards the center and

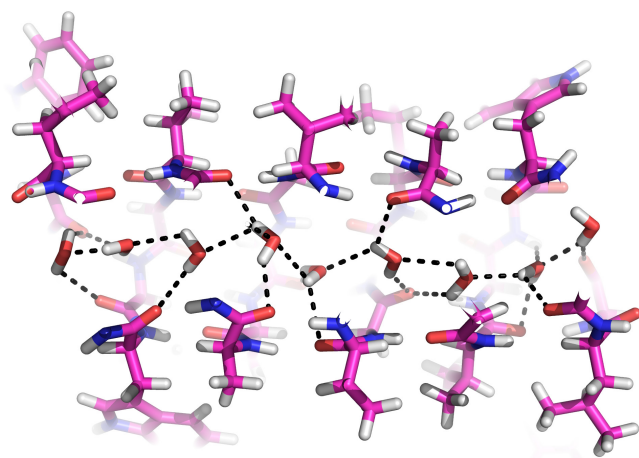


**Fig. 8.** Water molecules inside the gA channel taken from a single MD snapshot. The black dashed lines show hydrogen bonds between water molecules or between water molecules and the protein backbone carbonyls. This example has eight water molecules with seven water unique hydrogen bonds and 11 water:protein hydrogen bonds. The dipole moment of the eight water molecules in the gA channel is  $-15$  Debye.

the same number keep the oxygens pointing toward the outside of the channel (Fig. 7(b)). In the MCCE analysis the orientation with the oxygens pointing to the inside is preferred (Fig. 7(c)).

### 3.3. Hydrogen bond analysis of MD and MC simulations

Hydrogen bonds can be formed with neighboring water molecules or with the nearby protein backbone carbonyls (Fig. 8). The resultant number of hydrogen bonds have been compared for the restrained Classical MD simulation and MCCE simulation (Table 2). SSTMap was used to determine the average hydrogen bond number for each cluster.<sup>115</sup> This program divides all oxygen positions along the whole trajectory into eight clusters in a given MD frame or MC microstate (Fig. SI.10). The hydrogen bond connections between the specific water molecules found between water molecules assigned to a specific cluster in that frame or microstate are evaluated.

In the classical MD simulation, each water molecule has on average 1.60 hydrogen bonds with neighboring water molecules and 0.99 hydrogen bond with protein. These values are consistent with those found previously.<sup>20</sup> For the MCCE calculations there are only 0.61 hydrogen bonds with neighboring water molecules, fewer than MD. However, there are on average 1.22 hydrogen bonds to the protein which is more than the MD simulation.

The decrease in water:water hydrogen bonds in the MCCE calculations is a reflection of the less organized

**Table 2.** Average properties of water molecules in gA channel obtained from MCCE GCMC simulations and restrained MD trajectory with classical CHARMM36 force field.

Cluster	MC- $f_{\text{wat}}$	MC- $N_{\text{ww}}^{\text{HB}}$	MC- $N_{\text{pw}}^{\text{HB}}$	MD- $f_{\text{wat}}$	MD- $N_{\text{ww}}^{\text{HB}}$	MD- $N_{\text{pw}}^{\text{HB}}$
1	0.96	0.29	1.06	0.88	1.32	1.30
2	0.82	0.69	1.28	0.91	1.79	0.85
3	0.92	0.72	1.31	0.93	1.84	0.86
4	0.97	0.69	1.08	0.93	1.84	0.85
5	0.57	0.76	1.10	0.92	1.80	0.85
6	0.89	0.72	1.55	0.87	1.54	1.10
7	0.64	0.64	1.41	0.74	1.24	1.14
8	0.84	0.34	0.95	0.79	1.46	0.98
Mean	0.83	0.61	1.22	0.87	1.60	0.99
Std. Dev.	0.15	0.18	0.20	0.07	0.24	0.17

*Notes:* TIP3P water molecules are grouped into eight clusters as described in Section 8 (Supporting Information). SSTMap is used for the MD trajectory and the algorithm was repurposed to analyze the water molecules in each accepted MC microstate. The analysis of a MCCE simulation initiated with a single MD snapshot is shown.  $f_{\text{wat}}$ : Fraction of MD frames or MCCE snapshots that have a water in this cluster;  $N_{\text{ww}}^{\text{HB}}$ : Average number of hydrogen bonds between water molecules in this cluster with water molecules in adjacent clusters;  $N_{\text{pw}}^{\text{HB}}$ : Average number of hydrogen bonds between water molecules in the given cluster and the protein backbone. Mean and standard deviation average the properties of the eight clusters.

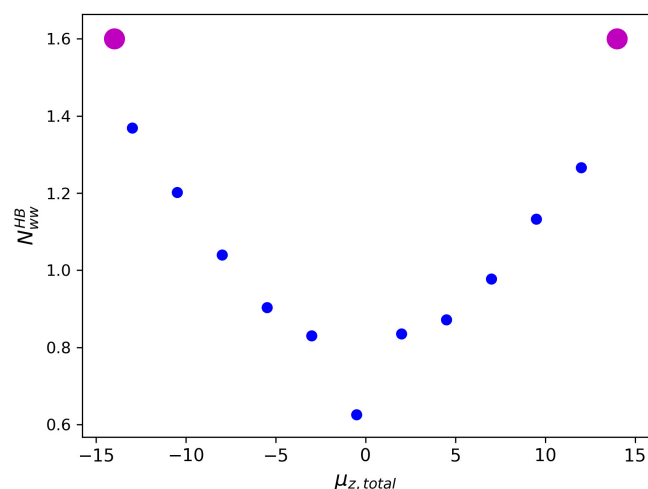


**Fig. 9.** (Color online) The number of hydrogen bonds between water molecules in MCCE microstates as a function of dipole moment of the microstate. MCCE microstates are binned into groups with the same dipole moment  $\pm 3D$ . Water molecules are divided into eight clusters as described in Table 2; Blue points: the average number of water:water hydrogen bonds between adjacent water clusters as a function of the microstate dipole moment; Purple points: average number of water:water hydrogen bonds between water clusters in the restrained MD trajectory.

water wires (Fig. 9). All MCCE microstates were divided by their summed dipole moments and the number of hydrogen bonds was determined for each microstate. The number of hydrogen bonds between water molecules increases as the water molecules become more aligned. When MD snapshots and MC

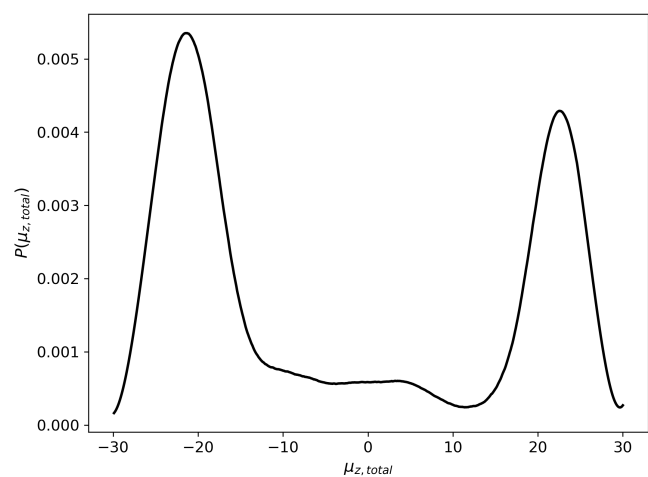


**Fig. 10.** The summed dipole moment distribution for enhanced water charge with water oxygen partial charge of  $-1.2$ . The MCCE analysis was initiated with the same MD snapshots and water positions as used in Fig. 6.

**Table 3.** Average properties of water molecules in gA channel obtained from MCCE GCMC simulations with O partial charge of  $-1.2$ .

Cluster	$f_{\text{wat}}$	$N_{ww}^{\text{HB}}$	$N_{pw}^{\text{HB}}$
1	0.84	0.66	1.00
2	0.92	1.39	1.32
3	0.98	1.58	0.94
4	0.99	1.86	0.35
5	0.97	1.91	1.64
6	0.99	1.60	1.61
7	0.92	0.92	1.26
8	0.37	0.58	0.74
Mean	0.87	1.31	1.11
Std. Dev.	0.21	0.53	0.44

*Note:* See Table 2 for a description of the table entries.

microstates have the same degree of alignment they have essentially the same number of water:water hydrogen bonds.

### 3.4. Increasing the water molecule atomic partial charges in MCCE

The MCCE parameters were modified, increasing the charge on the oxygen to be  $-1.2$ , to see if we could match the enhanced alignment of the water wires in the classical MD trajectory. In MCCE, the dielectric constant is 4, while it is 1 in the classical MD trajectory, thus the electrostatic screening reduces the interactions between the water molecules. Increasing the water partial charges increases the alignment of the MC water wire. The model with larger atomic partial charges has much larger total energies and proved to be much more difficult to come to convergence. A number of modifications were made for the MCCE MC sampling methods, which are described in Fig. SI.11. However, despite not being fully converged we present data on the system with large water partial charges because the properties of interest are found to be quite reproducible. The key result is with the larger charges the orientation of the water wire becomes significantly closer to that found in the classical MD trajectory (Fig. 10). As suggested in Fig. 9, the water wire becomes more oriented and more water:water hydrogen bonds are made (Table 3). Thus, with larger partial charges, the water wire orientation and hydrogen bond count approach that of the classical MD simulation.

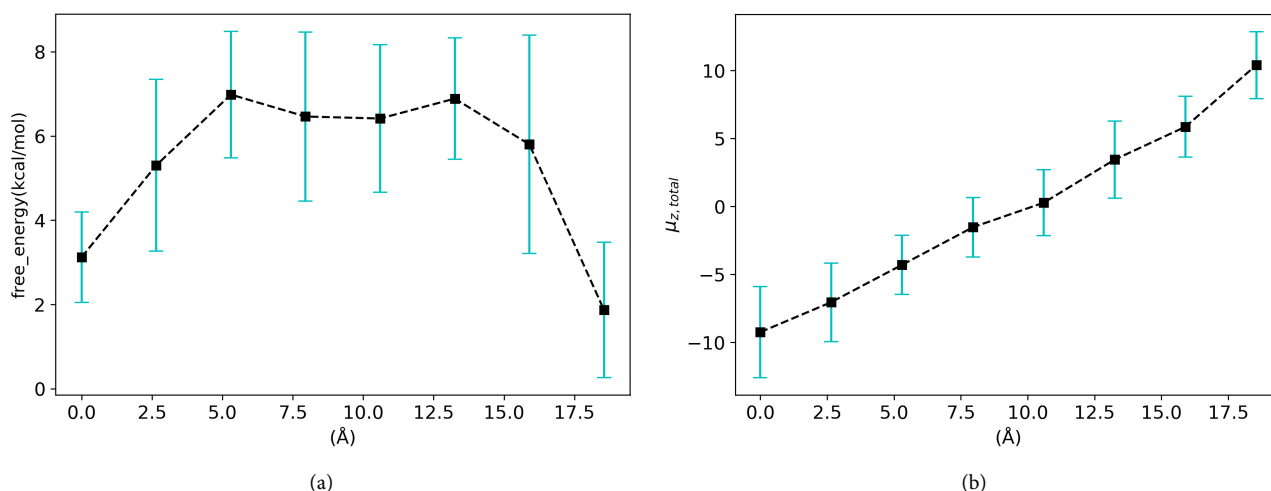


**Fig. 11.** (a) The free energy found for the gA channel with seven water molecules and one hydronium as a function of the hydronium position. The reference state has one hydronium in solution. (b) The dipole moment of the water wire as the hydronium is moved through the gA channel. The water wire is fully oriented with protons pointing away from the hydronium.

### 3.5. Barrier to hydronium transfer

The gA channel has been used as a model system for the study of ion and hydronium transfer through channels.<sup>98,119–121</sup> An excess proton is assumed to go through the channel via the Grotthuss mechanism.<sup>20,98,120</sup> To determine the energy of moving a hydronium through the channel in the MCCE simulation, we started with a microstate with eight water molecules within the 25 Å channel. One water at a time was replaced with a hydronium ( $\text{H}_3\text{O}^+$ ), which had five possible proton orientations. The protein structure and oxygen positions of water and hydronium are fixed. The proton positions on the hydronium and surrounding water molecules were allowed to come to equilibrium and the total system free energy was obtained. Thus, each calculation has seven water molecules and one hydronium. The results initiated with 10 different snapshots were averaged.

Generating hydronium from water in solution requires 12.36 kcal/mol at pH 7.4. The average barrier for moving a hydronium going through the channel is  $7.0 \pm 1.1$  kcal/mol (Fig. 11(a)). The value of the barrier for hydronium in the gA channel can be compared with earlier calculations which provided an estimate of 6 kcal/mol with an uncertainty of 1–2 kcal/mol<sup>44</sup> using the EVB model and Langevin dynamics to simulate the proton transportation in gA channel. The EVB simulations highlighted the importance of electrostatic energy in determining the proton transport rate. As CE/ME methods are optimized for the calculation of processes that change the charge state of the system, this may allow them to estimate the hydronium energy

using a classical model. In the presence of the hydronium all water molecules orient towards the positive charge (Fig. 11(b)).

## 4. CONCLUSION

Gramicidin is a simple water and cation conducting channel and so has provided a model system to explore the properties of water and ions in a confined space. We have investigated the ability of MCCE, which uses MC sampling with CE energies to recover the properties of water found with MD simulations. MD simulations without a polarizable force field yield a water wire with a single orientation through the channel. In contrast, with a polarizable Drude force field the water molecules have a summed dipole moment of the water molecules near zero. Thus, it is not certain what the water orientation in the gA channel should be.

MCCE with standard TIP3P water parameters yields water dipole orientations much closer to that found with the polarizable Drude MD simulation. This may reflect CE including polarization in the dielectric response. Increasing the charge on the water molecules in MCCE yields water orientations closer to that found in the nonpolarizable simulation. The barrier for hydronium in the channel of  $7 \pm 1$  kcal/mol calculated with MCCE, which agrees remarkably well with earlier calculations that used a more sophisticated EVB model.<sup>44</sup>

CE with implicit solvent is generally used to remove explicit water molecules, which have many degrees of freedom and can be difficult to come to equilibrium.

However, using gA as a model system, we see that explicit water molecules provide appropriate numbers of water molecules in the channel, degree of dipole orientation and barrier to hydronium found with other simulation techniques that use quite different methods of sampling and different force fields. This supports the use of hybrid continuum models that include explicit water in regions where they play a functional role, with implicit water elsewhere.

## ACKNOWLEDGMENTS

MG and YZ are supported by NSF MCB 1519640; TL by NSF MCB 1855942; SN and VN by the Natural Sciences and Engineering Research Council of Canada (NSERC) (Discovery Grant RGPIN-315019 to SYN) and the Alberta Innovates Technology Futures (AITF) Strategic Chair in BioMolecular Simulations through funding for Centre for Molecular Simulation. All calculations with polarizable force fields were performed on the CFI-supported TNK cluster at the University of Calgary and on the West-Grid/Compute Canada clusters under Research Allocation Award to SYN. The classical MD calculations used the resources of the OLCF at the Oak Ridge National Laboratory, which is supported by the Office of Science at DOE under Contract No. DE-AC05-00OR22725, made available via the INCITE program.

## References

1. Bellissent-Funel, M.-C.; Hassanali, A.; Havenith, M.; Henchman, R.; Pohl, P.; Sterpone, F.; van der Spoel, D.; Xu, Y.; Garcia, A. E. Water determines the structure and dynamics of proteins. *Chem. Rev.* **2016**, *116*, 7673–7697.
2. Ball, P. More than a bystander. *Nature* **2011**, *478*, 467–468.
3. Gunner, M.; Baker, N. Continuum electrostatics approaches to calculating pKas and Ems in proteins. *Meth. Enzymol.* **2016**, *578*, 1–20.
4. Mobley, D. L.; Gilson, M. K. Predicting binding free energies: Frontiers and benchmarks. *Annu. Rev. Biophys.* **2017**, *46*, 531–558.
5. Freier, E.; Wolf, S.; Gerwert, K. Proton transfer via a transient linear water-molecule chain in a membrane protein. *Proc. Natl. Acad. Sci.* **2011**, *108*, 11435–11439.
6. Goyal, P.; Lu, J.; Yang, S.; Gunner, M. R.; Cui, Q. Changing hydration level in an internal cavity modulates the proton affinity of a key glutamate in cytochrome c oxidase. *Proc. Natl. Acad. Sci. USA* **2013**, *110*, 18886–18891.
7. Cai, X.; Haider, K.; Lu, J.; Radic, S.; Son, C. Y.; Cui, Q.; Gunner, M. Network analysis of a proposed exit pathway for protons to the P-side of cytochrome c oxidase. *Biochim. Biophys. Acta. Bioenerg.* **2018**, *1859*, 997–1005.
8. Gunner, M. R.; Madeo, J.; Zhu, Z. Modification of quinone electrochemistry by the proteins in the biological electron transfer chains: Examples from photosynthetic reaction centers. *J. Bioenerg. Biomembr.* **2008**, *40*, 509–519.
9. Maupin, C. M.; Voth, G. A. Proton transport in carbonic anhydrase: Insights from molecular simulation. *Biochim. Biophys. Acta. Proteins Proteomics* **2010**, *1804*, 332–341.
10. Chamberlin, A.; Qiu, F.; Rebolledo, S.; Wang, Y.; Noskov, S. Y.; Larsson, H. P. Hydrophobic plug functions as a gate in voltage-gated proton channels. *Proc. Natl. Acad. Sci. USA* **2014**, *111*, E273–E282.
11. DeCoursey, T. E.; Hosler, J. Philosophy of voltage-gated proton channels. *J. R. Soc. Interface* **2014**, *11*, 20130799.
12. Lazaridis, T.; Hummer, G. Classical molecular dynamics with mobile protons. *J. Chem. Inf. Model* **2017**, *57*, 2833–2845.
13. van Keulen, S. C.; Gianti, E.; Carnevale, V.; Klein, M. L.; Rothlisberger, U.; Delemotte, L. Does proton conduction in the voltage-gated H<sup>+</sup> channel hHv1 involve grotthuss-like hopping via acidic residues? *J. Phys. Chem. B.* **2017**, *121*, 3340–3351.
14. Chenal, C.; Gunner, M. Two Cl Ions and a Glu Compete for a Helix Cage in the CLC Proton/Cl-Antiporter. *Biophys. J.* **2017**, *113*, 1025–1036.
15. Lee, S.; Mayes, H. B.; Swanson, J. M. J.; Voth, G. A. The origin of coupled chloride and proton transport in a Cl<sup>-</sup>/H<sup>+</sup> antiporter. *J. Am. Chem. Soc.* **2016**, *138*, 14923–14930.
16. Kelkar, D. A.; Chattopadhyay, A. The gramicidin ion channel: A model membrane protein. *Biochim. Biophys. Acta. Biomembr.* **2007**, *1768*, 2011–2025.
17. Li, H.; Anuwongcharoen, N.; Malik, A.; Prachayasittikul, V.; Wikberg, J.; Nantasenamat, C. Roles of D-amino acids on the bioactivity of host defense peptides. *Int. J. Mol. Sci.* **2016**, *17*, 1023.
18. Agmon, N.; Bakker, H. J.; Campen, R. K.; Henchman, R. H.; Pohl, P.; Roke, S.; Thämer, M.; Hassanali, A. Protons and hydroxide ions in aqueous systems. *Chem. Rev.* **2016**, *116*, 7642–7672.
19. Bozdaganyan, M. E.; Likhmatikov, A. V.; Voskobonnikova, N.; Cherepanov, D. A.; Steinhoff, H.-J.; Shaitan, K. V.; Mulikjanian, A. Y. Proton leakage across lipid bilayers: Oxygen atoms of phospholipid ester linkers align water molecules into transmembrane water wires. *Biochim. Biophys. Acta. Bioenerg.* **2019**, *1860*, 439–451.
20. Pomés, R.; Roux, B. Molecular mechanism of H<sup>+</sup> conduction in the single-file water chain of the Gramicidin channel. *Biophys. J.* **2002**, *82*, 2304–2316.

21. Rasaiah, J. C.; Garde, S.; Hummer, G. Water in non-polar confinement: From nanotubes to proteins and beyond. *Annu. Rev. Phys. Chem.* **2008**, *59*, 713–740.
22. Kopfer, D. A.; Song, C.; Gruene, T.; Sheldrick, G. M.; Zachariae, U.; de Groot, B. L. Ion permeation in K<sup>+</sup> channels occurs by direct Coulomb knock-on. *Science* **2014**, *346*, 352–355.
23. Kratochvil, H. T.; Carr, J. K.; Matulef, K.; Annen, A. W.; Li, H.; Maj, M.; Ostmeier, J.; Serrano, A. L.; Raghuraman, H.; Moran, S. D.; Skinner, J. L.; Perozo, E.; Roux, B.; Valiyaveetil, F. I.; Zanni, M. T. Instantaneous ion configurations in the K<sup>+</sup> ion channel selectivity filter revealed by 2D IR spectroscopy. *Science* **2016**, *353*, 1040–1044.
24. Ricci, M. A.; Bruni, F.; Gallo, P.; Rovere, M.; Soper, A. K. Water in confined geometries: Experiments and simulations. *J. Phys. Condens. Matter* **2000**, *12*, A345–A350.
25. Mann, D. J.; Halls, M. D. Water alignment and proton conduction inside carbon nanotubes. *Phys. Rev. Lett.* **2003**, *90*, 195503.
26. Jing, Z.; Liu, C.; Cheng, S. Y.; Qi, R.; Walker, B. D.; Piquemal, J.-P.; Ren, P. Polarizable force fields for biomolecular simulations: Recent advances and applications. *Annu. Rev. Biophys.* **2019**, *48*, 371–394.
27. Lemkul, J. A.; Huang, J.; Roux, B.; MacKerell, A. D. An empirical polarizable force field based on the classical Drude oscillator model: Development history and recent applications. *Chem. Rev.* **2016**, *116*, 4983–5013.
28. Lamoureux, G.; MacKerell, A. D.; Roux, B. A simple polarizable model of water based on classical Drude oscillators. *J. Chem. Phys.* **2003**, *119*, 5185–5197.
29. Ren, P.; Ponder, J. W. Polarizable atomic multipole water model for molecular mechanics simulation. *J. Phys. Chem. B* **2003**, *107*, 5933–5947.
30. Peng, X.; Zhang, Y.; Chu, H.; Li, Y.; Zhang, D.; Cao, L.; Li, G. Accurate Evaluation of ion conductivity of the Gramicidin A channel using a polarizable force field without any corrections. *J. Chem. Theory Comput.* **2016**, *12*, 2973–2982.
31. Xu, H.; Stern, H. A.; Berne, B. J. Can water polarizability be ignored in hydrogen bond kinetics? *J. Phys. Chem. B* **2002**, *106*, 2054–2060.
32. Leontyev, I. V.; Stuchebrukhov, A. A. Electronic polarizability and the effective pair potentials of water. *J. Chem. Theory Comput.* **2010**, *6*, 3153–3161.
33. Ngo, V. A.; Fanning, J. K.; Noskov, S. Y. Comparative analysis of protein hydration from MD simulations with additive and polarizable force fields. *Adv. Theory Simul.* **2019**, *2*, 1800106.
34. Huang, J.; Lopes, P. E. M.; Roux, B.; MacKerell, A. D. Recent advances in polarizable force fields for macromolecules: Microsecond simulations of proteins using the classical Drude oscillator model. *J. Phys. Chem. Lett.* **2014**, *5*, 3144–3150.
35. Takei, K.; Fang, H.; Kumar, S. B.; Kapadia, R.; Gao, Q.; Madsen, M.; Kim, H. S.; Liu, C.-H.; Chueh, Y.-L.; Plis, E.; Krishna, S.; Bechtel, H. A.; Guo, J.; Javey, A. Quantum confinement effects in nanoscale-thickness InAs membranes. *Nano Lett.* **2011**, *11*, 5008–5012.
36. Mosaddeghi, H.; Alavi, S.; Kowsari, M. H.; Najafi, B. Simulations of structural and dynamic anisotropy in nano-confined water between parallel graphite plates. *J. Chem. Phys.* **2012**, *137*, 184703.
37. Allen, T. W.; Andersen, O. S.; Roux, B. Ion permeation through a narrow channel: Using Gramicidin to ascertain all-atom molecular dynamics potential of mean force methodology and biomolecular force fields. *Biophys. J.* **2006**, *90*, 3447–3468.
38. Roux, B. Computational studies of the Gramicidin channel. *Acc. Chem. Res.* **2002**, *35*, 366–375.
39. Andersen, O. S.; Gramicidin channels. *Annu. Rev. Physiol.* **1984**, *46*, 531–548.
40. Allen, T. W.; Baştug, T.; Kuyucak, S.; Chung, S.-H. Gramicidin a channel as a test ground for molecular dynamics force fields. *Biophys. J.* **2003**, *84*, 2159–2168.
41. Basu, I.; Chattopadhyay, A.; Mukhopadhyay, C. Ion channel stability of Gramicidin A in lipid bilayers: Effect of hydrophobic mismatch. *Biochim. Biophys. Acta. Biomembr.* **2014**, *1838*, 328–338.
42. Allen, T. W.; Andersen, O. S.; Roux, B. Molecular dynamics potential of mean force calculations as a tool for understanding ion permeation and selectivity in narrow channels. *Biophys. Chem.* **2006**, *124*, 251–267.
43. Bransburg-Zabary, S.; Kessel, A.; Gutman, M.; Bent-Tal, N. Stability of an ion channel in lipid bilayers: Implicit solvent model calculations with Gramicidin. *Biochemistry* **2002**, *41*, 6946–6954.
44. Braun-Sand, S.; Burykin, A.; Chu, Z. T.; Warshel, A. Realistic simulations of proton transport along the Gramicidin channel: Demonstrating the importance of solvation effects. *J. Phys. Chem. B* **2005**, *109*, 583–592.
45. Gregory, J. K. The water dipole moment in water clusters. *Science* **1997**, *275*, 814–817.
46. Riniker, S. Fixed-charge atomistic force fields for molecular dynamics simulations in the condensed phase: An overview. *J. Chem. Inf. Model* **2018**, *58*, 565–578.
47. Baker, C. M. Polarizable force fields for molecular dynamics simulations of biomolecules. *WIREs Comput. Mol. Sci.* **2015**, *5*, 241–254.
48. Laury, M. L.; Wang, L.-P.; Pande, V. S.; Head-Gordon, T.; Ponder, J. W. Revised parameters for the AMOEBA polarizable atomic multipole water model. *J. Phys. Chem. B* **2015**, *119*, 9423–9437.
49. Fernández, D. P.; Mulev, Y.; Goodwin, A. R. H.; Sengers, J. M. H. L. A database for the static dielectric constant of water and steam. *J. Phys. Chem. Ref. Data* **1995**, *24*, 33–70.
50. Zasetky, A. Y. Dielectric relaxation in liquid water: Two fractions or two dynamics? *Phys. Rev. Lett.* **2011**, *107*, 117601.

51. Head-Gordon, T.; Paesani, F. Water is not a dynamic polydisperse branched polymer. *Proc. Natl. Acad. Sci. USA* **2019**, *116*, 13169–13170.
52. Jorgensen, W. L.; Chandrasekhar, J.; Madura, J. D.; Impey, R. W.; Klein, M. L. Comparison of simple potential functions for simulating liquid water. *J. Chem. Phys.* **1983**, *79*, 926–935.
53. Levy, R. M.; Gallicchio, E. Computer simulations with explicit solvent: Recent progress in the thermodynamic decomposition of free energies and in modeling electrostatic effects. *Annu. Rev. Phys. Chem.* **1998**, *49*, 531–567.
54. Morawietz, T.; Singraber, A.; Dellago, C.; Behler, J. How van der Waals interactions determine the unique properties of water. *Proc. Natl. Acad. Sci. USA* **2016**, *113*, 8368–8373.
55. Qiu, Y.; Nerenberg, P. S.; Head-Gordon, T.; Wang, L.-P. Systematic optimization of water models using liquid/vapor surface tension data. *J. Phys. Chem. B* **2019**, *123*, 7061–7073.
56. Zhang, H.; Yin, C.; Jiang, Y.; van der Spoel, D. Force field benchmark of amino acids: hydration and diffusion in different water models. *J. Chem. Inf. Model* **2018**, *58*, 1037–1052.
57. Best, R. B.; Mittal, J. Protein simulations with an optimized water model: Cooperative helix formation and temperature-induced unfolded state collapse. *J. Phys. Chem. B* **2010**, *114*, 14916–14923.
58. Nerenberg, P. S.; Jo, B.; So, C.; Tripathy, A.; Head-Gordon, T. Optimizing solute–water van der Waals interactions to reproduce solvation free energies. *J. Phys. Chem. B* **2012**, *116*, 4524–4534.
59. Ashbaugh, H. S.; Collett, N. J.; Hatch, H. W.; Staton, J. A. Assessing the thermodynamic signatures of hydrophobic hydration for several common water models. *J. Chem. Phys.* **2010**, *132*, 124504.
60. Levy, R. M.; Zhang, L. Y.; Gallicchio, E.; Felts, A. K. On the Nonpolar hydration free energy of proteins: Surface area and continuum solvent models for the solute–solvent interaction energy. *J. Am. Chem. Soc.* **2003**, *125*, 9523–9530.
61. Feig, M.; Brooks, C. L. Recent advances in the development and application of implicit solvent models in biomolecule simulations. *Curr. Opin. Struct. Biol.* **2004**, *14*, 217–224.
62. Onufriev, A. V.; Case, D. A. Generalized born implicit solvent models for biomolecules. *Annu. Rev. Biophys.* **2019**, *48*, 275–296.
63. Ross, G. A.; Bodnarchuk, M. S.; Essex, J. W. Water sites, networks, and free energies with grand canonical Monte Carlo. *J. Am. Chem. Soc.* **2015**, *137*, 14930–14943.
64. Barillari, C.; Taylor, J.; Viner, R.; Essex, J. W. Classification of water molecules in protein binding sites. *J. Am. Chem. Soc.* **2007**, *129*, 2577–2587.
65. Nielsen, J. E.; Gunner, M. R.; Garca-Moreno, E. B. The pKa cooperative: A collaborative effort to advance structure-based calculations of pKa values and electrostatic effects in proteins. *Proteins* **2011**, *79*, 3249–3259.
66. Machuqueiro, M.; Baptista, A. M. Is the prediction of pKa values by constant-pH molecular dynamics being hindered by inherited problems? *Proteins* **2011**, *79*, 3437–3447.
67. Radak, B. K.; Chipot, C.; Suh, D.; Jo, S.; Jiang, W.; Phillips, J. C.; Schulten, K.; Roux, B. Constant-pH molecular dynamics simulations for large biomolecular systems. *J. Chem. Theory Comput.* **2017**, *13*, 5933–5944.
68. Swails, J. M.; York, D. M.; Roitberg, A. E. Constant pH replica exchange molecular dynamics in explicit solvent using discrete protonation states: Implementation, testing, and validation. *J. Chem. Theory Comput.* **2014**, *10*, 1341–1352.
69. Cruzeiro, V. W. D.; Amaral, M. S.; Roitberg, A. E. Redox potential replica exchange molecular dynamics at constant pH in AMBER: Implementation and validation. *J. Chem. Phys.* **2018**, *149*, 072338.
70. Baker, N. A. Improving implicit solvent simulations: A Poisson-centric view. *Curr. Opin. Struct. Biol.* **2005**, *15*, 137–143.
71. Gilson, M. K.; Rashin, A.; Fine, R.; Honig, B. On the calculation of electrostatic interactions in proteins. *J. Mol. Biol.* **1985**, *184*, 503–516.
72. Leontyev, I.; Stuchebrukhov, A. Accounting for electronic polarization in non-polarizable force fields. *Phys. Chem. Chem. Phys.* **2011**, *13*, 2613.
73. Gunner, M. R.; Zhu, X.; Klein, M. C. MCCE analysis of the pKas of introduced buried acids and bases in staphylococcal nuclease. *Proteins* **2011**, *79*, 3306–3319.
74. Sham, Y. Y.; Muegge, I.; Warshel, A. The effect of protein relaxation on charge-charge interactions and dielectric constants of proteins. *Biophys. J.* **1998**, *74*, 1744–1753.
75. Csnyi, V.; Boda, D.; Gillespie, D.; Kristf, T. Current and selectivity in a model sodium channel under physiological conditions: Dynamic Monte Carlo simulations. *Biochim Biophys Acta Biomembr* **2012**, *1818*, 592–600.
76. Song, Y.; Gunner, M. Using multiconformation continuum electrostatics to compare chloride binding motifs in  $\alpha$ -amylase, human serum albumin, and Omp32. *J. Mol. Biol.* **2009**, *387*, 840–856.
77. Till, M. S.; Essigke, T.; Becker, T.; Ullmann, G. M. Simulating the proton transfer in Gramicidin A by a sequential dynamical Monte Carlo Method. *J. Phys. Chem. B* **2008**, *112*, 13401–13410.
78. Song, Y.; Mao, J.; Gunner, M. R. MCCE2: Improving protein pKa calculations with extensive side chain rotamer sampling. *J. Comput. Chem.* **2009**, 2231–2247.
79. Song, Y.; Mao, J.; Gunner, M. R. Calculation of proton transfers in bacteriorhodopsin bR and Mintermediates. *Biochemistry* **2003**, *42*, 9875–9888.

80. Song, Y.; Gunner, M. R. Halorhodopsin pumps  $\text{Cl}^-$  and bacteriorhodopsin pumps protons by a common mechanism that uses conserved electrostatic interactions. *Proc. Natl. Acad. Sci. USA* **2014**, *111*, 16377–16382.
81. Zheng, Z.; Dutton, P. L.; Gunner, M. R.; The measured and calculated affinity of methyl- and methoxy-substituted benzoquinones for the Q(A) site of bacterial reaction centers. *Proteins* **2010**, *78*, 2638–2654.
82. Hassanali, A. A.; Cuny, J.; Verdolino, V.; Parrinello, M. Aqueous solutions: State of the art in *ab initio* molecular dynamics. *Philos. Trans. R. Soc. A* **2014**, *372*, 20120482.
83. Warshel, A. *Computer modeling of chemical reactions in enzymes and solutions*, Wiley, New York, **1991**.
84. Voth, G. A. Computer simulation of proton solvation and transport in aqueous and biomolecular systems. *Acc. Chem. Res.* **2006**, *39*, 143–150.
85. Knight, C.; Voth, G. A. The curious case of the hydrated proton. *Acc. Chem. Res.* **2012**, *45*, 101–109.
86. Stillinger, F. H.; David, C. W. Polarization model for water and its ionic dissociation products. *J. Chem. Phys.* **1978**, *69*, 1473–1484.
87. Weber, T. A.; Stillinger, F. H. Dynamical study of the  $\text{H}_5\text{O}_2^+ + \text{H}_3\text{O}_2^-$  neutralization reaction using the polarization model. *J. Chem. Phys.* **1982**, *77*, 4150–4155.
88. Ojamae, L.; Shavitt, I.; Singer, S. J. Potential models for simulations of the solvated proton in water. *J. Chem. Phys.* **1998**, *109*, 5547–5564.
89. Lussetti, E.; Pastore, G.; Smargiassi, E. A fully polarizable and dissociable potential for water. *Chem. Phys. Lett.* **2003**, *381*, 287–291.
90. Mahadevan, T. S.; Garofalini, S. H. Dissociative water potential for molecular dynamics simulations. *J. Phys. Chem. B* **2007**, *111*, 8919–8927.
91. van Duin, A. C. T.; Zou, C.; Joshi, K.; Bryantsev, V.; Goddard, W. A.; in Asthagiri, A.; Janik, M. J. (eds.), A reaxff reactive force-field for proton transfer reactions in bulk water and its applications to heterogeneous catalysis, *Catalysis Series*; Royal Society of Chemistry, Cambridge, 223–243, **2013**.
92. Lill, M. A.; Helms, V. Molecular dynamics simulation of proton transport with quantum mechanically derived proton hopping rates (Q-HOP MD). *J. Chem. Phys.* **2001**, *115*, 7993–8005.
93. Wolf, M.; Grubmüller, H.; Groenhof, G. Anomalous surface diffusion of protons on lipid membranes. *Biophys. J.* **2014**, *107*, 76–87.
94. Kong, X.; Brooks, C. L.  $\lambda$ -dynamics: A new approach to free energy calculations. *J. Chem. Phys.* **1996**, *105*, 2414–2423.
95. Wolf, M. G.; Groenhof, G. Explicit proton transfer in classical molecular dynamics simulations. *J. Comput. Chem.* **2014**, *35*, 657–671.
96. Pomés, R.; Roux, B. Free energy profiles for  $\text{H}^+$  conduction along hydrogen-bonded chains of water molecules. *Biophys. J.* **1998**, *75*, 33–40.
97. Marrink, S.; Jhng, F.; Berendsen, H. Proton transport across transient single-file water pores in a lipid membrane studied by molecular dynamics simulations. *Biophys. J.* **1996**, *71*, 632–647.
98. Swanson, J. M. J.; Maupin, C. M.; Chen, H.; Petersen, M. K.; Xu, J.; Wu, Y.; Voth, G. A. Proton solvation and transport in aqueous and biomolecular systems: Insights from computer simulations. *J. Phys. Chem. B* **2007**, *111*, 4300–4314.
99. Jo, S.; Kim, T.; Iyer, V. G.; Im, W. CHARMM-GUI: A web-based graphical user interface for CHARMM. *J. Comput. Chem.* **2008**, *29*, 1859–1865.
100. Bowers, K. J.; Chow, D. E.; Xu, H.; Dror, R. O.; Eastwood, M. P.; Gregersen, B. A.; Klepeis, J. L.; Kolossvary, I.; Moraes, M. A.; Sacerdoti, F. D.; Salmon, J. K.; Shan, Y.; Shaw, D. E. Scalable algorithms for molecular dynamics simulations on commodity clusters, *ACM/IEEE SC 2006 Conference (SC'06)*, Tampa, FL; pp. 43–43, **2006**.
101. Lamoureux, G.; Harder, E.; Vorobyov, I. V.; Roux, B.; MacKerell, A. D. A polarizable model of water for molecular dynamics simulations of biomolecules. *Chem. Phys. Lett.* **2006**, *418*, 245–249.
102. Lopes, P. E. M.; Huang, J.; Shim, J.; Luo, Y.; Li, H.; Roux, B.; MacKerell, A. D. Polarizable force field for peptides and proteins based on the classical Drude oscillator. *J. Chem. Theory Comput.* **2013**, *9*, 5430–5449.
103. Luo, Y.; Jiang, W.; Yu, H.; MacKerell, A. D.; Roux, B. Simulation study of ion pairing in concentrated aqueous salt solutions with a polarizable force field. *Faraday Discuss* **2013**, *160*, 135–149.
104. Yu, H.; Whitfield, T. W.; Harder, E.; Lamoureux, G.; Vorobyov, I.; Anisimov, V. M.; MacKerell, A. D.; Roux, B. Simulating monovalent and divalent ions in aqueous solution using a Drude polarizable force field. *J. Chem. Theory Comput.* **2010**, *6*, 774–786.
105. Ngo, V.; Li, H.; MacKerell Jr, A. D.; Allen, T. W.; Roux, B.; Noskov, S. Polarization effects in water-mediated selective cation transport across a narrow transmembrane channel, *Submitted*.
106. Phillips, J. C.; Braun, R.; Wang, W.; Gumbart, J.; Tajkhorshid, E.; Villa, E.; Chipot, C.; Skeel, R. D.; Kal, L.; Schulten, K. Scalable molecular dynamics with NAMD. *J. Comput. Chem.* **2005**, *26*, 1781–1802.
107. Allen, T. W.; Andersen, O. S.; Roux, B. Structure of Gramicidin A in a lipid bilayer environment determined using molecular dynamics simulations and solid-state NMR data. *J. Am. Chem. Soc.* **2003**, *125*, 9868–9877.
108. Jiang, W.; Hardy, D. J.; Phillips, J. C.; MacKerell, A. D.; Schulten, K.; Roux, B. High-performance scalable molecular dynamics simulations of a polarizable force

- field based on classical Drude oscillators in NAMD. *J. Phys. Chem. Lett.* **2011**, *2*, 87–92.
109. Lamoureux, G.; Roux, B. Modeling induced polarization with classical Drude oscillators: Theory and molecular dynamics simulation algorithm. *J. Chem. Phys.* **2003**, *119*, 3025–3039.
  110. Sprik, M. Computer simulation of the dynamics of induced polarization fluctuations in water. *J. Phys. Chem.* **1991**, *95*, 2283–2291.
  111. Gunner, M. R.; Murakami, T.; Rustenburg, A. S.; Isik, M.; Chodera, J. D. Standard state free energies, not pK<sub>a</sub>s, are ideal for describing small molecule protonation and tautomeric states. *J. Comput-Aided Mol. Des.* **2020**, *34*, 561–573.
  112. Honig, B.; Sharp, K.; Yang, A. S. Macroscopic models of aqueous solutions: Biological and chemical applications. *J. Phys. Chem.* **1993**, *97*, 1101–1109.
  113. Sitkoff, D.; Sharp, K. A.; Honig, B. Accurate calculation of hydration free energies using macroscopic solvent models. *J. Phys. Chem.* **1994**, *98*, 1978–1988.
  114. Pearlman, D. A.; Case, D. A.; Caldwell, J. W.; Ross, W. S.; Cheatham, T. E.; DeBolt, S.; Ferguson, D.; Seibel, G.; Kollman, P. AMBER, a package of computer programs for applying molecular mechanics, normal mode analysis, molecular dynamics and free energy calculations to simulate the structural and energetic properties of molecules. *Comput. Phys. Commun.* **1995**, *91*, 1–41.
  115. Haider, K.; Cruz, A.; Ramsey, S.; Gilson, M. K.; Kurtzman, T. Solvation structure and thermodynamic mapping (SSTMap): An open-source, flexible package for the analysis of water in molecular dynamics trajectories. *J. Chem. Theory Comput.* **2018**, *14*, 418–425.
  116. Humphrey, W.; Dalke, A.; Schulten, K. VMD: Visual molecular dynamics. *J. Mol. Graphics* **1996**, *14*, 33–38.
  117. Horner, A.; Pohl, P. Single-file transport of water through membrane channels. *Faraday Discuss* **2018**, *209*, 9–33.
  118. Sitkoff, D.; Sharp, K. A.; Honig, B. Correlating solvation free energies and surface tensions of hydrocarbon solutes. *Biophys. Chem.* **1994**, *51*, 397–409.
  119. Allen, T. W.; Andersen, O. S.; Roux, B. Energetics of ion conduction through the gramicidin channel. *Proc. Natl. Acad. Sci.* **2004**, *101*, 117–122.
  120. Lee, M.; Bai, C.; Feliks, M.; Alhadeff, R.; Warshel, A. On the control of the proton current in the voltage-gated proton channel Hv1. *Proc. Natl. Acad. Sci. USA* **2018**, *115*, 10321–10326.
  121. Setiadi, J.; Kuyucak, S. Computational investigation of the effect of lipid membranes on ion permeation in Gramicidin A. *Membranes* **2016**, *6*, 20.